Dipolar collisions of polar molecules in the quantum regime

K.-K. Ni,[1*] S. Ospelkaus,[1*] D. Wang,[1] G. Quéméner,[1] B. Neyenhuis,[1]
M. H. G. de Miranda,[1] J. L. Bohn,[1] J. Ye,[1†] D. S. Jin[1†]

[1] *JILA, NIST and University of Colorado,*
Department of Physics,
University of Colorado
Boulder, CO 80309-0440, USA

[*] *These authors contributed equally to this work;*

[†] *To whom correspondence should be addressed;*
E-mail: Ye@jila.colorado.edu; Jin@jilau1.colorado.edu

PACS numbers:

Ultracold polar molecules offer the possibility of exploring quantum gases with interparticle interactions that are strong, long-range, and spatially anisotropic. This is in stark contrast to the much studied dilute gases of ultracold atoms, which have isotropic and extremely short-range, or "contact", interactions. Furthermore, the large electric dipole moment of polar molecules can be tuned with an external electric field; this provides unique opportunities such as the control of ultracold chemical reactions [1], a unique platform for quantum information processing [2–4], and the realization of novel quantum many-body systems [5–8]. In spite of intense experimental efforts aimed at observing the influence of dipoles on ultracold molecules [9], only recently have sufficiently high densities been achieved [10]. Here, we report the experimental observation of dipolar collisions in an ultracold molecular gas prepared close to quantum degeneracy. For modest values of an applied electric field, we observe a dramatic increase in the loss rate of fermionic KRb molecules due to ultrcold chemical reactions. We find that the loss rate has a steep power-law dependence on the induced electric dipole moment, and we show that this dependence can be understood with a relatively simple model based on quantum threshold laws for scattering of fermionic polar molecules. In addition, we directly observe the spatial anisotropy of the dipolar interaction as manifested in measurements of the thermodynamics of the dipolar gas. These results demonstrate how the long-range dipolar interaction can be used for electric-field control of chemical reaction rates in an ultracold polar molecule gas. Furthermore, the large loss rates in an applied electric field suggest that creating a long-lived ensemble of ultracold polar molecules may require confinement in a two-dimensional trap geometry in order to suppress the influence of the attractive head-to-tail dipolar interactions [11–14].

Dipolar interactions have been explored in several atom gas experiments using the magnetic dipole moments of atoms [15, 16], however this interaction is intrinsically orders of magnitude weaker than the dipolar interaction between typical polar molecules. Ultracold gases of polar molecules, then, open the possibility for realizing strong, and therefore relatively long-range, interactions. For example, with polar molecules confined in optical lattice potentials, one could realize a system where the interactions between particles in neighboring

sites is as strong as the on-site interactions now commonly realized with atoms. This longer range interaction for polar molecules will allow access to a new regime of strongly correlated quantum gases with unique phase transitions, such as to supersolid phases for bosons [17, 18] and to topological superfluid phases for fermions [19]. Another important difference between magnetic and electric dipolar interactions is that the strength of the effective electric dipole moment is tunable with an applied electric field. In addition to its obvious utility for controlling the interaction strength in dipolar quantum gases, the electric-field dependence could be exploited in the development of novel quantum computing schemes or in the control of ultracold chemical reactions.

We perform our experiments with an ultracold gas of ^{40}K^{87}Rb molecules prepared in a single nuclear hyperfine state within the ro-vibronic ground state ($^1\Sigma^+$) [10, 20]. The gas is confined in a pancake-shaped optical dipole trap, which is realized by overlapping two horizontally propagating, elliptically shaped laser beams with a wavelength of $\lambda = 1064\,\mathrm{nm}$. Typical harmonic trapping frequencies are $\omega_\mathrm{x} = 2\pi \times 40$ Hz and $\omega_\mathrm{z} = 2\pi \times 280$ Hz, in the horizontal and vertical directions, respectively. The KRb molecules have a permanent electric dipole moment of 0.57 Debye [10], where 1 Debye $= 3.336 \times 10^{-30}$ C m. However, the effective molecular dipole moment in the lab frame is zero in the absence of an external electric field. When an external electric field is applied, the molecules begin to align with the field, and have an induced dipole moment, d, that increases as shown in the inset of Fig. 1 B. This figure covers the range of applied electric field that we currently access experimentally, which corresponds to an accessible dipole moment range of 0 to 0.22 Debye. In our setup, the external electric field points in the vertical direction ($\hat{z}$), parallel to the tight axis of the optical trap. Thus, the spatially anisotropic dipolar interactions will be predominantly repulsive for molecules colliding in the horizontal direction (side-by-side) and predominantly attractive for molecules approaching each other along the vertical direction (head-to-tail).

In an ultracold gas, the quantum statistics of the particles plays an essential role in the interactions. Our ^{40}K^{87}Rb molecules are fermions prepared in a single internal quantum state at a temperature equal to 1.4 times the Fermi temperature. Therefore, the quantum statistics requires that the wave function for two colliding molecules be antisymmetric with respect to molecule exchange. If one considers the relative angular momentum between two colliding molecules, this means that scattering can only proceed via odd partial waves, and will be dominated by angular momentum $L = 1$ (p-wave) scattering at ultralow tempera-

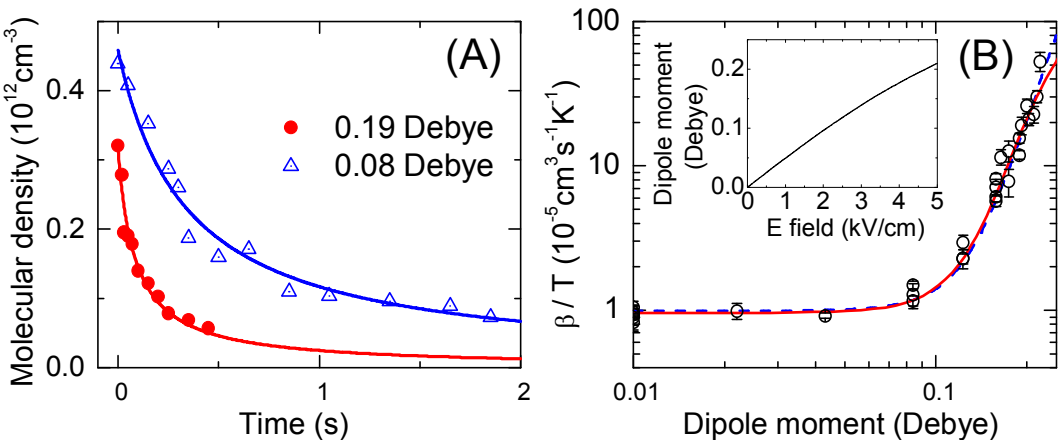

FIG. 1: Two-body inelastic loss for fermionic polar molecules. (A) We extract the inelastic loss rate coefficient β from a fit (solid lines) to the measured time evolution of the trapped molecular gas density. The data shown here are for an induced dipole moment $d = 0.08$ Debye (open triangles) and $d = 0.19$ Debye (filled circles), and an initial temperature $T = 300$ nK. (B) We plot β, divided by T, as a function of the induced dipole moment, d. A fit to a power-law dependence in the region $d > 0.1$ Debye yields a power of 6.1 ± 0.8. The dashed line shows a fit to a simple model based on the quantum threshold behavior for tunneling through a dipolar-interaction modified p-wave barrier (see text). The solid line shows the result of a more complete quantum scattering calculation including an absorbing potential at short range. Note that the full model (dashed line) deviates from the simple model prediction at our largest d where the scattering is no longer in the Wigner threshold regime. The calculated dependence of the induced dipole moment on the applied electric field is shown in the inset to (B).

ture. Previous work at zero electric field (without long-range dipolar interactions) showed that the lifetime of the trapped ^{40}K^{87}Rb molecules is limited by atom-exchange chemical reactions that proceed via p-wave scattering [21]. In our experiments, the typical translational temperature of the molecular gas is 300 nK, while the energy height of the p-wave barrier for ^{40}K^{87}Rb molecules corresponds to a temperature of approximately 24 μK [22]. With the barrier height much larger than typical collision energies, scattering rates in the molecular cloud are determined by the tunneling rate through the centrifugal barrier and the molecular gas lifetime is relatively long (on the order of 1 s) [21].

In this paper, we investigate the effect of electric dipolar interactions on collisions and find a surprisingly large effect even for our relatively modest range of applied electric fields.

We measure the molecular loss rate by monitoring the time evolution of the average number density of trapped molecules, n (see Fig. 1 A). We fit the data to the solution of

$$\frac{dn}{dt} = -\beta n^2 - \alpha n, \tag{1}$$

shown as solid lines in Fig. 1 A.

The first term on the right hand side accounts for number loss, and we extract the measured two-molecule inelastic loss rate coefficient, β, (which is two times the collisional event rate) from the fit. The second term describes density change arising from heating of the trapped gas during the measurement. In a single measurement, we observe an increase in temperature that is at most 50%. In subsequent analysis, we fit the measured temperature to a linear heating and obtain a constant slope c. In Eqn. 1, we then use $\alpha = \frac{3}{2}\frac{c}{T+ct}$, where T is the initial temperature of the gas (see also [21]).

Fig. 1 B shows a summary of our experimental data, where we plot β/T, as a function of d. We plot the ratio β/T because the Wigner threshold law for p-wave scattering predicts that β scales linearly with T, and we previously verified this temperature dependence at $d = 0$ Debye [21]. For the data in Fig. 1, T ranged from 250 nK to 500 nK. In Fig. 1 B we see that dipolar interactions have a dramatic effect on the inelastic collision rate. At low electric field, where d is below 0.1 Debye, we observe no significant modification to the zero electric-field loss rate (which is plotted at $d = 0.01$ Debye for inclusion on the logarithmic scale). However, for higher electric fields, we observe a rapidly increasing loss rate, with well over an order of magnitude increase in β/T by $d = 0.2$ Debye. Fitting the data for $d > 0.1$ Debye, we find that the inelastic rate coefficient follows a power-law dependence on d, $\beta/T \propto d^p$, where $p = 6.1 \pm 0.8$.

To understand this strong electric-field dependence of the inelastic loss rate, we consider a relatively simple quantum tunneling model where the loss is assumed to be due to collisions between fermionic molecules that proceed via tunneling through a p-wave centrifugal barrier followed by unit probability for loss at short-range [14]. The fact that we do not observe any resonant oscillations as a function of E-field (see Fig. 1 B) is consistent with a very high loss probability for molecules reaching short range. In an applied electric field, the long-range dipole-dipole interaction $\propto \frac{1}{R^3}$, where R is the intermolecular separation, significantly modifies the height of the p-wave barrier, and thus changes the inelastic collision rate. Moreover, the fact that the dipole-dipole interaction is spatially anisotropic means that

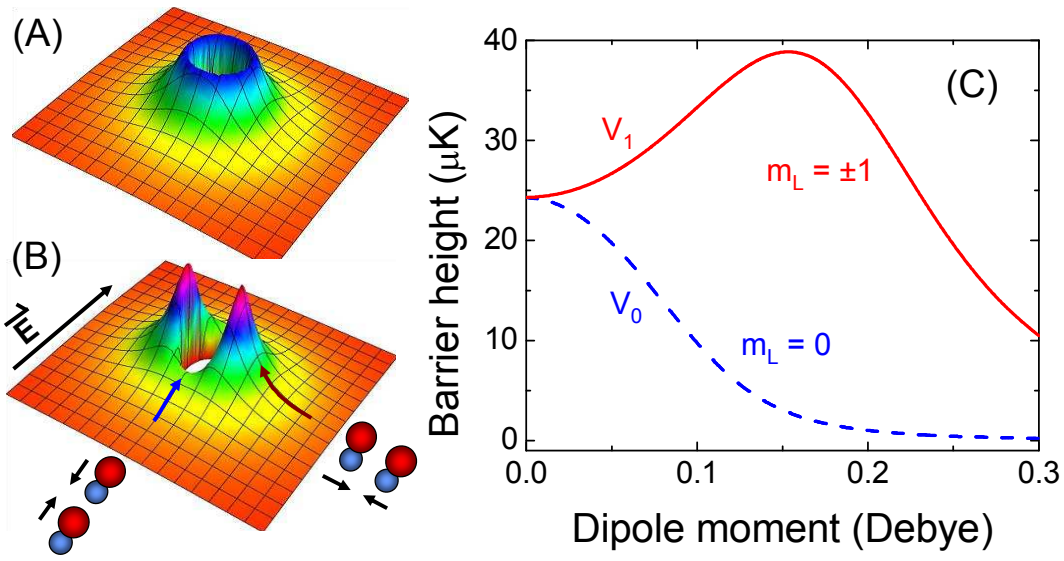

FIG. 2: p-wave centrifugal barrier for dipolar collisions between fermionic polar molecules. (A) Schematic picture of the effective intermolecular potential for fermionic molecules at zero electric field. At intermediate intermolecular separation (center of plot), two colliding molecules are repelled by a large centrifugal barrier for p-wave collisions. (B) Schematic picture of the effective intermolecular potential for a relatively small applied electric field. The dipolar interactions are spatially anisotropic, with an attraction that reduces the barrier for head-to-tail collisions and a repulsion that increases the barrier for side-by-side collisions. (C) Height of the p-wave barrier as a function of dipole moment for repulsive dipole-dipole interactions (V_1, solid red line) and for attractive dipole-dipole interactions (V_0, dashed blue line). As the induced dipole moment increases, the spatially anisotropic dipolar interactions lower the centrifugal barrier for $m_L = 0$ collisions and raise the barrier for $m_L = \pm 1$ collisions. The lowering of the $m_L = \pm 1$ barrier at very large dipole moments is due to mixing with higher partial waves, e.g. $L = 3, 5, 7, ...$

the p-wave barrier height will be different for $m_L = 0$ and $m_L = \pm 1$ scattering, where m_L is the projection of the relative orbital angular momentum L onto the electric-field direction. In particular, the attractive nature of dipole-dipole interaction for polar molecules colliding "head-to-tail" lowers the barrier for $m_L = 0$ collisions, while the repulsive dipole-dipole interaction for polar molecules colliding "side-by-side" raises the barrier for $m_L = \pm 1$ collisions. Fig. 2 A,B show these effects schematically, while Fig. 2 C shows the calculated maximum height of the $m_L = 0$ and $m_L = \pm 1$ collisional barriers, V_0 and V_1, respectively, as a function of d.

In our simple model, we assume that the collision rate follows the Wigner threshold law for p-wave inelastic collisions, namely $\beta \propto T/V_{0,1}^{3/2}$. For large d, V_0 is significantly smaller than V_1, and the loss will proceed predominantly through "head-to-tail" attractive collisions of the polar molecules. In this regime, V_0 scales as d^{-4} and the model predicts that β/T will increase with a characteristic power law of d^6 for $d > 0.1$ Debye [14]. This prediction is in excellent agreement with our measured dependence of the loss rate on d for $d > 0.1$ Debye (Fig. 1 B).

For a quantitative description of the inelastic collisional rate over our full range of experimentally accessible dipole moments, we include contributions from both $m_L = 0$ and $m_L = \pm 1$ collisions, and we calculate the barrier heights using adiabatic potential curves that include mixing with higher partial waves (see Fig. 2 C). We fit the prediction of this quantum threshold model to our data using a scaling factor, γ, as a free fit parameter, where γ can be interpreted as the loss probability when the collision energy equals the height of the barrier. The resulting theoretical prediction (solid line in Fig. 1) agrees very well with our experimental data (open circles), and we obtain $\gamma = 0.35 \pm 0.08$. However, in order to get this agreement over the full range of d, we found it necessary to introduce a second fit parameter that multiplies the coefficient, C_6, of the van-der-Waals interaction. The best fit value of this parameter is 1.9 ± 0.9. Also shown in Fig. 1 B as a dashed line is the result of a more complete quantum scattering calculation that employs a strong absorptive potential at short range but captures the long-range physics and uses C_6 as the single fit parameter. This fit also agrees well with the experimental data, and gives $C_6 = 21000 \pm 7000$ a.u. in good agreement with the predicted value of $C_6 = 16130$ a.u. [22].

Accompanying the increased inelastic loss rates for increasing d, we observe an increased heating rate for the polar molecule gas. In Fig. 3 we plot the measured initial heating rate as a function of d. The heating rate $\dot{T} = c$ is extracted using a linear fit to the measured molecular cloud temperature vs. time, over a time period sufficiently long to allow T to increase by approximately 20 to 30%. In Fig 3, we plot the fractional heating rate $\dot{T}/T$ normalized by both the initial n and the initial T. We have developed a simple thermodynamic model for heating that is directly caused by the inelastic loss. We consider the energy lost from the gas when molecules are removed in inelastic collisions, and assume that the gas stays in thermal equilibrium. In this model (see Supplementary Information), the heating arises solely from an"anti-evaporation" mechanism in the trap [23, 24], where

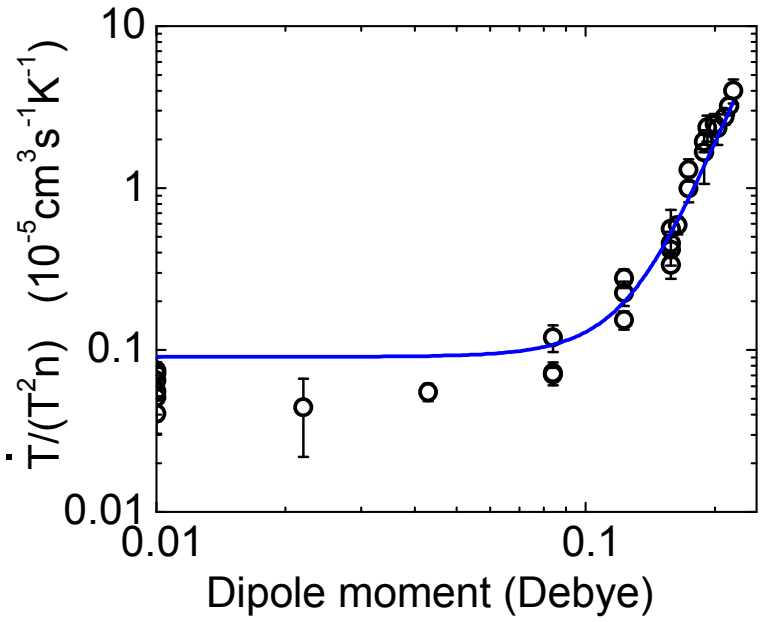

FIG. 3: Normalized fractional heating rate $\frac{\dot{T}}{T}/(Tn)$ as a function of dipole moment. The heating rate is extracted using a linear fit to the initial temperature increase and is then normalized by the initial density and temperature of the ensemble. The line is the expected heating rate given by $\dot{T}/(T^2n) = (\beta/T)/12$ (see text). Typical initial conditions for these data are $n = 0.3 \cdot 10^{12}/$ cm^3 and $T = 0.5$ μK, and the absolute heating rate ranges from 0.1 μK/s at zero electric field to 2 μK/s at our largest electric fields.

the particles removed by inelastic collisions have, on average, lower energies than typical particles in the gas. One way to understand this heating mechanism is simply to note that inelastic collisions preferentially remove particles from the center of the trap where the number density is the highest, and where the particles have the lowest potential energy from the trap. We also include in our calculations a competing "cooling"effect that comes from the fact that the p-wave inelastic collision rate increases linearly with the collision energy. Including these two competing effects, we obtain $\dot{T}/(T^2n) = (\beta/T)/12$ (see Supplementary Information). Remarkably, this simple prediction, Fig. 3 (solid line), using the β/T values from the fit to our loss rate data in Fig. 1 with no additional free parameter, agrees very well with the independently measured heating rates for the molecule gas.

The anisotropy of the dipole-dipole interaction is directly revealed in an anisotropic distribution of molecules in the trap. The average energy per particle, which we measure from the expansion of the gas following a sudden release from the trap, can be different in the

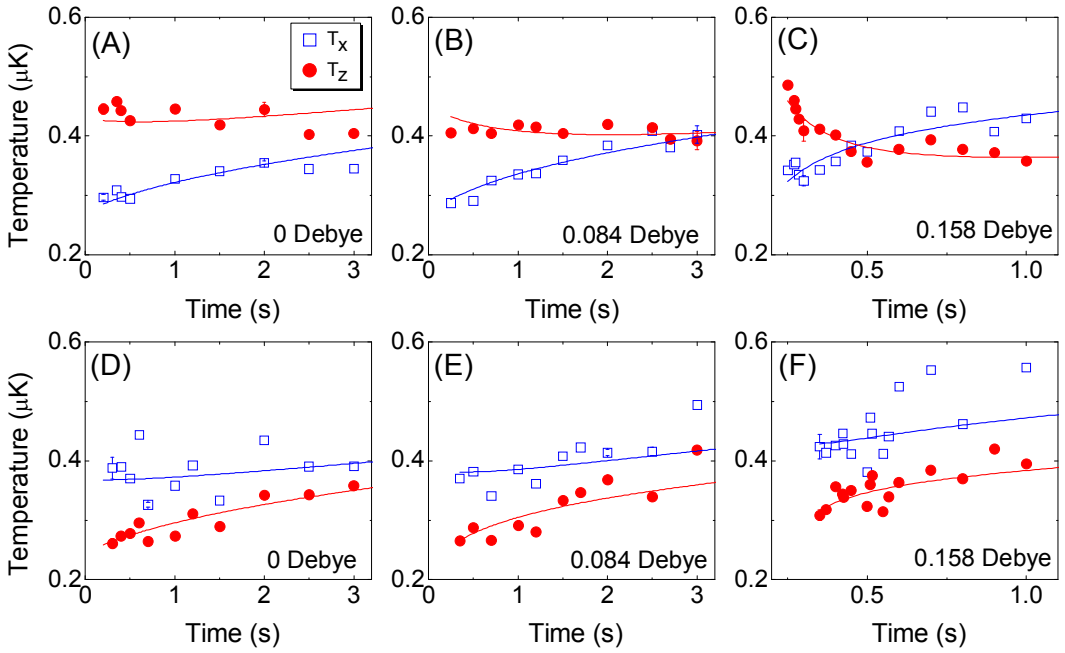

FIG. 4: Apparent cross-dimensional rethermalization as a function of dipole moment for $T_z > T_x$ (upper row, A-C) and $T_z < T_x$ (lower row, D-F) in the polar molecule gas. The experimental data reveal a striking difference between the results for heating the gas in the vertical direction (A to C) and heating in the horizontal directions (D to F), and thus provide evidence for the strong anisotropic characteristic of dipolar interactions (see text). The electric field is applied along $\hat{z}$.

vertical and horizontal directions. In the following, we present measurements of the time evolution of the expansion energy in the two directions for different d. To probe the spatial anisotropy of dipolar collisions, we start by adding energy along one direction of the cylindrically symmetric trap using parametric heating. Here, we modulate the power of both optical trapping beams at twice the relevant harmonic trapping frequency for 50 ms (z-direction) or 100 ms (x,y-directions). We then wait 100 ms before quickly increasing the electric field (in less than 1μs) to the desired final value and measuring the time dependence of the vertical (T_z) and horizontal (T_x) "temperatures" of the cloud. Here, T_z and T_x simply correspond to the measured expansion energies in the two directions. We note that this type of measurement is commonly used in ultracold atom gas experiments to measure the elastic collision cross section [25].

Figure 4 shows the experimental data for these rethermalization experiments with three values of d and under two initial conditions: $T_z > T_x$ (upper row, A-C) and $T_z < T_x$ (lower

row, D-F). For $d = 0$ Debye (Fig. 4 A and D), T_z and T_x equilibrate very slowly on a timescale of approximately 4 s. Because $d = 0$ Debye, there are no dipolar interactions and the data agree with our expectation of very slow equilibration for spin-polarized fermions. Indeed, this is the longest rethermalization time we have observed in our trap, and therefore the data are consistent with no elastic collisions and only technical imperfections such as a small cross-dimensional coupling in the trapping potential.

In an applied electric field, the elastic collision cross section due to long-range dipolar interactions is predicted to increase as d^4 [26]. For the case where initially $T_z > T_x$ (Fig. 4 B,C), our data show that T_z and T_x approach each other, in what appears at a casual glance to be cross-dimensional rethermalization. The timescale for this apparent rethermalization even decreases steeply with increasing d as one might expect. However, we note that in Fig. 4 C the temperatures cross each other at long times, which is inconsistent with rethermalization driven by elastic collisions. Even more striking is the fact that the thermodynamic behavior of the gas is completely different when the gas initially has $T_z < T_x$. In this case, T_z and T_x do not equilibrate during the measurement time (see Fig. 4 E,F).

The explanation for these surprising observations comes from the spatially anisotropic nature of inelastic dipole-dipole collisions and the fact that the molecule gas experiences number loss. We have seen (Fig. 3) that loss due to inelastic collisions heats the gas, and we can quantitatively understand this heating rate by considering the effect of molecule loss on the average energy per particle. We can adapt the heating and inelastic collision model described above to allow the average energy per particle, or "temperature", to be different in the two trap directions. The "anti-evaporation" picture then predicts that the dominant head-to-tail collisions ($m_L = 0$) will lead to heating in x and y but cooling along z. Side-by-side collisions ($m_L = \pm 1$), on the other hand, should contribute to heating along z but give no temperature change in x and y (see Methods and Supplementary Information). To compare this model to our rethermalization-type data, we fix the d-dependent β using the fit to our data in Fig. 1 (solid line). This fixes both the time evolution of the molecule number as well as the heating rates in the two trap directions. We then accommodate possible elastic collision effects in the model by adding a term that would exponentially drive the energy difference between the two directions to zero. Figure 4 shows a comparison between the results of the model (solid lines) and our experimental data. Although the model uses few free parameters (only the elastic collision cross-section, in addition to the initial n, T_x, and

T_z), it provides excellent agreement with the experimental data.

Our observations provide clear evidence of the anisotropic nature of the dipole-dipole interactions through the observed anisotropy in the apparent rethermalization. From the agreement of the data with the model, we conclude that the rethermalization behavior is actually dominated by the anisotropic nature of the inelastic collisions. What then can we conclude about elastic collisions? The best fit value for the elastic collision cross section is finite and increases with increasing d. This is consistent with the prediction that the elastic collision rate for polar molecules will scale as d^4 [26], and, furthermore, the fit values agree with the prediction of cross sections on the order of $\sigma_{\rm el} = 7 \cdot 10^{-8}{\rm cm}^2/({\rm s\ Debye}^4)$ [26]. However, the presence of inelastic loss and the resulting anisotropic heating make it difficult to accurately extract a measured value of the elastic cross section for a more precise comparison with theory.

The results presented here demonstrate that modest applied electric fields can dramatically alter the interactions of fermionic polar molecules in the quantum regime. For future efforts aimed at studying many-body phenomena in dipolar molecular quantum systems it will be necessary to protect the gas from strong inelastic loss and heating [11, 12, 27]. In particular, the demonstration here of strong spatial anisotropy for inelastic collisions of polar molecules suggests that going to a two-dimensional trapped gas will be a promising route to realizing a long-lived quantum gas of polar molecules with dipole-dipole interactions. This could be achieved, for example, with polar molecules confined in an array of 2D pancakes in a 1D optical lattice trap [11, 12]. Interestingly, even when short-range inelastic loss processes are suppressed, the attractive part of the long-range dipole-dipole interaction could still give rise to correlations between neighboring 2D pancakes in the 1D lattice trap [28, 29].

A. Methods

For the fit to a quantum threshold model [14] in Fig. 1 B, we write the inelastic loss rate coefficient, $\beta = K_0 T_z + 2K_1 T_x$, as the sum of two terms corresponding to $m_L = 0$ and $m_L = \pm 1$ scattering, respectively, and we assume $T_z = T_x = T$. The d-dependent coefficients, K_0 and K_1 are obtained using

$$K_{0,1} = \gamma \frac{3\,\pi\,\hbar^2}{\sqrt{2\mu^3} V_{0,1}^{3/2}}\ k_B, \tag{2}$$

where $\hbar = \frac{h}{2\pi}$, h is Planck's constant, and k_B is the Boltzmann constant. The barrier heights, V_0 and V_1, are taken to be the maximum energy of the long-range adiabatic potential $V(R)$ evaluated in a basis set of partial waves $|LM_L\rangle$ [14]. The potential $V(R)$ includes a repulsive centrifugal term, $\hbar^2 L(L+1)/(2\mu R^2)$ where μ is the reduced mass of the colliding molecules, an attractive isotropic van der Waals interaction $-bC_6/R^6$, and the dipolar interaction. We use only two fit parameters, b and γ, when fitting this model to the measured β/T vs. d.

The solid lines in Fig. 4 are a fit of the measured time evolution of n, T_z, and T_x to the numerical solution of three differential equations (see Supplementary Information):

$$\frac{dn}{dt} = -(K_0 T_z + 2K_1 T_x)n^2 - \frac{n}{2T_z}\frac{dT_z}{dt} - \frac{n}{T_x}\frac{dT_x}{dt} \tag{3}$$

$$\frac{dT_z}{dt} = \frac{n}{4}(-K_0 T_z + 2K_1 T_x)T_z - \frac{2\Gamma_{el}}{3}(T_z - T_x) + c_{bg} \tag{4}$$

$$\frac{dT_x}{dt} = \frac{n}{4}(K_0 T_z)T_x + \frac{\Gamma_{el}}{3}(T_z - T_x) + c_{bg} \tag{5}$$

Here, we have allowed for a difference in the average energy per particle in the two trap directions, "T_z" and "T_x", so that $\beta = K_0 T_z + 2K_1 T_x$. For the fits, we fix the d-dependent coefficients K_0 and K_1 using the previous fit to the inelastic loss rate data in Fig. 1. In addition to heating due to inelastic loss, we include a measured background heating rate of $c_{bg} = 0.01$ μK/s. The elastic collision rate in Eqns. 4 and 5 is given by $\Gamma_{el} = \frac{n\sigma_{el}v}{N_{coll}}$, where the elastic collision cross section σ_{el} is a fit parameter, $v = \sqrt{\frac{8k_B(T_z+2T_x)}{3\pi\mu}}$, and the constant N_{coll} can be thought of as the mean number of collisions per particle required for rethermalization. We use $N_{coll} = 4.1$, which was computed for p-wave collisions [30], however, we note that N_{coll} depends on the angular dependence of the scattering and may be somewhat different for dipolar elastic collisions.

[1] Krems, R. V. Perspective: Cold Controlled Chemistry. *Phys. Chem. Chem. Phys.* **10**, 4079 (2008).

[2] DeMille, D. Quantum Computation with Trapped Polar Molecules. *Phys. Rev. Lett.* **88,** 067901 (2002).

[3] Andre, A., DeMille, D., Doyle, J. M., Lukin, M. D., Maxwell, S. E., Rabl, P., Schoelkopf, R. J., Zoller, P. A coherent all-electrical interface between polar molecules and mesoscopic superconducting resonators. *Nature Physics* **2,** 636-642 (2006).

[4] Yelin, S. F., Kirby, K., Côte, R. Schemes for robust quantum computation with polar molecules. *Phys. Rev. A* **74,** 050301 (2006).

[5] Micheli, A., Brennen, G. K., Zoller, P. A toolbox for lattice-spin models with polar molecules. *Nat. Phys.* **2**, 341-347 (2006).

[6] Lahaye, T., Menotti, C., Santos, L., Lewenstein, M., Pfau, T. The physics of dipolar bosonic quantum gases *Rep. Prog Phys.* **72,** 126401 (2009).

[7] Pupillo, G., Micheli, A., Büchler, H. P., Zoller, P. Condensed Matter Physics with Cold Polar Molecules. in *Cold Molecules: Theory, Experiment, Applications*, ed. Krems, R. V., Stwalley, W. C., Friedrich, B. (CRC Press, Boca Raton, FL, 2009).

[8] Baranov, M. Theoretical progress in many-body physics with ultracold dipolar gases. *Phys. Rep.* **464**, 71-111 (2008).

[9] Carr, L. D., DeMille, D., Krems, R. V., Ye. J. Cold and ultracold molecules: science, technology and applications. *New J. Phys.* **11**, 055049 (2009).

[10] Ni, K.-K. *et al.* A High-Phase-Space-Density Gas of Polar Molecules. *Science* **322**, 231 (2008).

[11] Micheli, A. *et al.* Cold polar molecules in two-dimensional traps: Tailoring interactions with external fields for novel quantum phases. *Phys. Rev. A* **76,** 043604 (2007).

[12] Büchler, H. P. *et al.* Strongly correlated 2D quantum phases with cold polar molecules: Controlling the shape of the interaction potential. *Phys. Rev. Lett.* **98,** 060404 (2007).

[13] Li, Z., Krems, R. V. Inelastic collisions in an ultracold quasi-two-dimensional gas. *Phys. Rev. A* **79**, 050701 (2009).

[14] Quéméner, G., Bohn, J. L. Strong Dependence of Ultracold Chemical Rates on Electric Dipole Moments. *Phys. Rev. A* in press (2009).

[15] Stuhler, J. *et al.* Observation of Dipole-Dipole Interaction in a Degenerate Quantum Gas. *Phys. Rev. Lett.* **95**, 150406 (2005).

[16] Vengalattore, M., Leslie, S. R., Guzman, J., Stamper-Kurn, D. M. *et al.* Spontaneously modulated spin textures in a dipolar spinor Bose-Einstein condensate. *Phys. Rev. Lett.* **100**, 170403 (2008).

[17] Gral, K., Santos, L., Lewenstein, M. Quantum Phases of Dipolar Bosons in Optical Lattices. *Phys. Rev. Lett.* **88**, 170406 (2002).

[18] Capogrosso-Sansone, B., Trefzger, C., Lewenstein, M., Zoller, P., Pupillo, G. Quantum Phases of Cold Polar Molecules in 2D Optical Lattices (2009) Preprint at

http://arxiv.org/abs/0906.2009.

[19] Cooper, N. R., Shlyapnikov, G. V. Stable Topological Superfluid Phase of Ultracold Polar Fermionic Molecules *Phys. Rev. Lett.* **103**, 155302 (2009).

[20] Ospelkaus, S. *et al.* Controlling the Hyperfine State of Rovibronic Ground State Polar Molecules. *Phys. Rev. Lett.* in press (2009). Preprint at http://arxiv.org/abs/0908.3931.

[21] Ospelkaus, S. *et al.* Quantum-State Controlled Chemical Reactions of Ultracold KRb Molecules. *Science*, in press (2009).

[22] Kotochigova, S. private communication (2009).

[23] Roberts, J. L. Bose-Einstein Condensates with Tunable Atom-atom Interactions. PhD diss., University of Colorado (2001).

[24] Weber, T., Herbig, J., Mark, M., Nägerl, H.-C., Grimm, R. Three-Body Recombination at Large Scattering Lengths in an Ultracold Atomic Gas. *Phys. Rev. Lett.* **91**, 123201 (2003).

[25] Monroe, C. R., Cornell, E. A., Sackett, C. A., Myatt, C. J., Wieman, C. E. Measurement of Cs-Cs elastic scattering at T=30 μK. *Phys. Rev. Lett.* **70**, 414 (1993).

[26] Bohn, J. L., Cavagnero, M., Ticknor, C. Quasi-universal dipolar scattering in cold and ultracold gases. *New J. Phys.* **11**, 055039 (2009).

[27] Gorshkov, A. V. *et al.* Suppression of inelastic collisions between polar molecules with a repulsive shield. *Phys. Rev. Lett.* **101** 073201 (2008).

[28] Wang, D. W., Lukin, M. D., Demler, E. Quantum fluids of self-assembled chains of polar molecules. *Phys. Rev. Lett.* **97,** 180413 (2006).

[29] Klawunn, M., Duhme, J., Santos, L. Bose-Fermi mixtures of self-assembled filaments of fermionic polar molecules. arXiv:0907.4612 (2009).

[30] DeMarco, B., Bohn, J. L., Burke, Jr., J. P., Holland, M. H., Jin, D. S. Measurement of p-wave threshold law using evaporatively cooled fermionic atoms. *Phys. Rev. Lett.* **82**, 4208 (1999).

Supplementary Information is linked to the online version of the paper at www.nature.com/nature.

Supporting online material

Heating due to two-body inelastic p-wave collisions

Loss of trapped atoms or molecules due to inelastic collisions gives rise to heating through a mechanism called "anti-evaporation", where particles removed from the trap have, on average, a lower energy than the remaining particles. Here, we model the heating due to inelastic two-body p-wave collisional loss in a trapped gas, as relevant to our experiments.

To accommodate the spatial anisotropy of the dipole-dipole interaction and the possibility of an anisotropic energy distribution in the trapped gas, we define "temperatures" along three spatial directions using

$$T_i = \frac{E_i}{k_B N}, \tag{1}$$

where the index $i = x, y, z$ and N is the number of molecules. As the trap shape is a flat disk perpendicular to the vertical (z) axis, which is also the direction of the electric field, it is natural to assume that the temperatures in the two radial trap directions, T_x and T_y, are equal. The energies E_i are defined as

$$\begin{aligned} E_z &= \sum \left(\frac{1}{2} m v_z^2 + \frac{1}{2} m \omega_z z^2 \right) \\ E_x &= \sum \left(\frac{1}{2} m v_x^2 + \frac{1}{2} m \omega_x x^2 \right), \end{aligned} \tag{2}$$

where m is the particle mass, ω_z and ω_r are the axial and radial trapping frequencies, respectively, and the sum is taken over all particles in the trap. The heating rates are then given by

$$\frac{dT_i}{dt} = -\frac{T_i}{N}\frac{dN}{dt} + \frac{1}{k_B N}\frac{dE_i}{dt}. \tag{3}$$

Each two-body inelastic collision removes two particles, so the loss rate is given by

$$\frac{dN}{dt} = -2N\Gamma_{coll}, \tag{4}$$

where Γ_{coll} is the inelastic collision rate per particle. Similarly,

$$\frac{dE_i}{dt} = -\Delta E_i N \Gamma_{coll}, \tag{5}$$

where ΔE_i is the average E_i for a pair of particles that is lost from the trap. Putting this together, we have

$$\frac{dT_i}{dt} = 2T_i\Gamma_{coll} - \frac{\Delta E_i}{k_B}\Gamma_{coll}. \tag{6}$$

To find the heating caused by inelastic collisional loss we need to calculate ΔE_z and ΔE_x. The total energy of any pair of particles is the sum of four terms: kinetic and potential energy of the center-of-mass motion of the two colliding particles, and their relative kinetic and potential energy. In any of the three directions, the ensemble average for the energy is $2k_BT$ with equal contributions ($1/2k_BT$) coming from each of the four terms. However, the average energy for pairs of particles that undergo inelastic collisions is, in general, different from the ensemble average because the collision rate depends on the relative position and relative velocity. Because collisions are only sensitive to relative motion, the kinetic and potential energy of the center-of-mass motion of the two colliding particles will be on average the same as the ensemble average, ($1/2k_BT$). The relative potential energy is zero for colliding particles (since they must be at the same position to collide). This is the reason that collisional loss in a trap leads to"anti-evaporative" heating, in contrast to the elastic-collision-based evaporative cooling where energetic particles are preferentially removed from a trap.

It remains then to consider the relative kinetic energy. For p-wave inelastic collisions, the collision rate increases linearly with the relative energy of the colliding particles. Furthermore, as discussed in the main text, the spatial anisotropy of the dipole-dipole interaction can result in different rates for $m_L = 0$ and $m_L = \pm 1$ collisions. Therefore, we calculate the heating for $m_L = 0$ and $m_L = \pm 1$ collisions separately and then add the heating rates in the final result. For $m_L = 0$ collisions, we find the average relative energy for two colliding particles using

$$\begin{aligned} E^0_{z,rel} &= \frac{1}{2}\mu\frac{\int_{-\infty}^{\infty} f(v_z, v_r) v_z^4 dv_z}{\int_{-\infty}^{\infty} f(v_z, v_r) v_z^2 dv_z} \\ &= \frac{3}{2}k_B T_z \end{aligned} \tag{7}$$

$$\begin{aligned} E^0_{x,rel} &= \frac{1}{4}\mu\frac{\int_{0}^{\infty} f(v_z, v_r) v_r^2 (2\pi v_r) dv_r}{\int_{0}^{\infty} f(v_z, v_r) (2\pi v_r) dv_r} \\ &= \frac{1}{2}k_B T_x \end{aligned} \tag{8}$$

where we assume a Maxwell-Boltzmann distribution of relative velocities given by

$$f(v_z, v_r) \propto \exp\left(-\frac{\mu v_r^2}{2k_B T_r}\right) \exp\left(-\frac{\mu v_z^2}{2k_B T_z}\right) \tag{9}$$

with $v_r^2 = v_x^2 + v_y^2$. A factor of v_z^2 in both the numerator and denominator of Eqn. (7) accounts for the fact that the $m_L = 0$ p-wave inelastic collision rate scales as collision energy $\propto v_z^2$. Similarly, for $m_L = \pm 1$ collisions, the collision rate scales as v_r^2 and we find the average relative energy for two colliding particles using

$$\begin{aligned} E^1_{z,rel} &= \frac{1}{2}\mu \frac{\int_{-\infty}^{\infty} f(v_z, v_r) v_z^2 dv_z}{\int_{-\infty}^{\infty} f(v_z, v_r) dv_z} \\ &= \frac{1}{2} k_B T_z \end{aligned} \tag{10}$$

$$\begin{aligned} E^1_{x,rel} &= \frac{1}{4}\mu \frac{\int_0^{\infty} f(v_z, v_r) v_r^4 (2\pi v_r) dv_r}{\int_0^{\infty} f(v_z, v_r) v_r^2 (2\pi v_r) dv_r} \\ &= k_B T_x. \end{aligned} \tag{11}$$

Adding this to the $k_B T_i$ from the center-of-mass energies, we get

$$\Delta E^0_z = \frac{5}{2} k_B T_z \tag{12}$$

$$\Delta E^0_x = \frac{3}{2} k_B T_x \tag{13}$$

$$\Delta E^1_z = \frac{3}{2} k_B T_z \tag{14}$$

$$\Delta E^1_x = 2 k_B T_x. \tag{15}$$

Putting this into the expression for the heating rate (Eqn. (6)), we find that

$$\frac{dT_z}{dt} = -\frac{1}{2} T_z \Gamma^0_{coll} + \frac{1}{2} T_z \Gamma^1_{coll} \tag{16}$$

$$\frac{dT_x}{dt} = +\frac{1}{2} T_x \Gamma^0_{coll}. \tag{17}$$

In the main text, we defined the loss rate coefficient as

$$\begin{aligned} \beta &= K_0 T_z + 2 K_1 T_x \\ &= \frac{2}{n}\left(\Gamma^0_{coll} + \Gamma^1_{coll}\right), \end{aligned} \tag{18}$$

where K_0 and K_1 depend on the induced dipole moment. The inelastic collision rate per particle is related to β through

$$\Gamma^0_{coll} = \frac{K_0 T_z n}{2} \tag{19}$$

$$\Gamma^1_{coll} = \frac{2 K_1 T_x n}{2}. \tag{20}$$

With this substitution, our final result for the heating due to inelastic loss is

$$\frac{dT_z}{dt} = \frac{n}{4}(-K_0 T_z + 2K_1 T_x)T_z \tag{21}$$

$$\frac{dT_x}{dt} = \frac{n}{4}(K_0 T_z)T_x. \tag{22}$$

If we assume that the ensemble stays in cross-dimensional equilibrium, $T = T_z = T_x$, then the overall heating rate is simply

$$\begin{aligned} \frac{dT}{dt} &= \frac{1}{3}\frac{dT_z}{dt} + \frac{2}{3}\frac{dT_x}{dt} \\ &= \frac{n}{12}(K_0 + 2K_1)T^2, \end{aligned} \tag{23}$$

or equivalently,

$$\frac{dT}{dt}/(T^2 n) = \frac{\beta/T}{12}. \tag{24}$$